Proceedings of the 17th International Modal Analysis Conference, Kissimmee, FL, Feb. 8-11, 1999.

APPLICATION OF RITZ VECTORS TO DAMAGE DETECTION FOR A GRID-TYPE BRIDGE MODEL

Hoon Sohn and Kincho H. Law

Department of Civil and Environmental Engineering
Stanford University
Stanford, CA 94305-4020

ABSTRACT

This paper describes an experimental study on the use of Ritz vectors for damage detection of a grid-type bridge model. A new procedure to extract Ritz vectors from experimental modal analysis is proposed and demonstrated using the test structure. Using appropriate load patterns, Ritz vectors can be made more sensitive to damage than modal vectors. The results indicate that the use of load-dependent Ritz vectors produce better damage diagnoses than the modal vectors.

1 INTRODUCTION

Damage detection and health monitoring of large-scale structures are important challenges to engineering research. One common approach is to employ the vibration characteristics of a structure to predict the damage locations and to estimate the amount of damage [4]. It has been shown that changes in the modal parameters might not be apparent at an early stage of damage [5, 7]. Also, the uncertainties caused by measurement noise, modeling error involved in an analytical model, and environmental changes such as variations in temperature and load conditions can impede reliable identification of damage [6]. Therefore, for reliable damage detection, damage would need to cause significant changes in the modal parameters that are beyond the natural variability caused by the effects other than damage.

To overcome the insensitivity of modal vectors, several alternatives have been proposed. Pandey, Biswas, and Samman [9] compute the mode shape curvature from the displacement mode shape, and demonstrate that the changes in the mode shape curvature can be a good indicator of damage for beam structures. Stubbs, Kim and Topole [12] present a damage index method which measures the decrease of modal strain energy before and after damage occurrence. Yao, Chang and Lee [13] apply the strain mode shape to identify local damage detection of a braced steel frame structure. The idea is that the force redistribution caused by damage can be related to the change of the strain mode shape. These methods require the direct measurement of dynamic strains or the derivatives of the measured displacement mode shapes to compute the strain mode shape or mode shape curvature. However, the noise induced by the measurement of dynamic strains is generally higher than that by typical accelerometer measurement. Furthermore, numerical procedures to compute the curvature from the displacement also inevitably produce errors. Ritz vectors (or Lanczos vectors) have been shown very effective for dynamic and earthquake analyses, eigenvalue problems and model reductions. However, very few studies have applied Ritz vectors to damage detection or system identification problems [1, 8, 11]. Recently, Cao and Zimmerman [2] show that it is possible to experimentally extract Ritz vectors from the traditional modal analysis.

In this paper, Ritz vectors are incorporated into the previously proposed Bayesian probabilistic framework [10] and the applicability is investigated using a grid-type bridge model constructed and tested at the Hyundai Institute of Construction Technology (HICT), Korea (see Figure 1). We also present a new extraction procedure of Ritz vectors based on a measured flexibility matrix. The estimated Ritz vectors are then applied to perform the damage diagnosis for the test structure.

2 EXPERIMENTAL BRIDGE MODEL

The steel bridge test model consists of two parallel girders and six evenly spaced cross beams connecting the two girders as shown in Figure 1. The girders are steel rectangular tubes and the cross beams are C-shape members. Using impact excitations, we extract Ritz/modal vectors from the vibration response of the test structure.

A SA-390 signal analyzer with four channels is used for the analog to digital conversion of accelerometer signals and the Fast Fourier Transform (FFT) calculation. Data acquisition parameters are specified such that a frequency response func-

Figure 1: An overview of a grid-type bridge structure

tion (FRF) in the range of 0 to 100 Hz could be estimated. Each spectrum is computed by averaging three 8 second long time histories. 2048 points are sampled for a 8 second time period and this sampling rate produces a frequency resolution of 0.125 Hz. An exponential window is applied to all measured time histories prior to the FFT calculation.

A Dytran 5801A4 impact hammer and three Dytran 3100B accelerometers with a normal sensitivity of 100mV/g are used. The excitation is applied to nodes 3, 4 and 5 as shown in Figure 2. The sensors measure the vertical accelerations at the twelve nodes as indicated in Figure 2.

Note that since the SA-390 data acquisition system has only four channels and there are three accelerometers, the first channel is always connected to the input hammer and the remaining three channels are connected to three accelerometers. To complete one set of modal test, the hammer excitation is repeated twelve times at one point and the three accelerometers are moved from one set of three nodes to another set of three nodes after every three excitations (note that each FRF is computed by averaging the three response time histories, and there are twelve measurement points and three accelerometers).

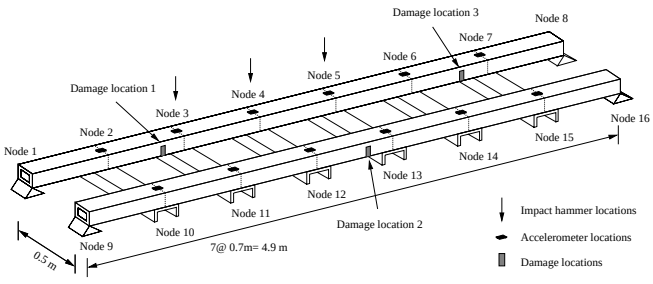

Figure 2: Impact, accelerometer and damage locations of the grid-type bridge structure

The DIAMOND [1] software developed by the Los Alamos National Laboratory is employed for the extraction of modal parameters. The ERA and rational polynomial techniques are employed to extract the first six natural frequencies and the corresponding modal vectors from the recorded FRFs.

3 FLEXIBILITY BASED EXTRACTION OF RITZ VECTORS

Cao and Zimmerman [2] proposed a procedure to extract Ritz vectors based on the state-space matrices estimated from vibration tests. In this section, we present a new extraction procedure of Ritz vectors based on a measured flexibility matrix. A close look at the analytical generation procedure in Reference 2 reveals that the generation of Ritz vectors uses the flexibility matrix $\mathbf{F}$ (defined here as the inverse of the stiffness matrix) rather than the stiffness matrix itself.

The extraction of Ritz vectors starts with the assumption that the dynamic loading $\mathbf{F}(s,t)$ can be separated into a spatial load vector $\mathbf{f}(s)$and time function $u(t)$:

$$\mathbf{F}(s,t) = \mathbf{f}(s)u(t) \tag{1}$$

If the modal vectors are mass-normalized such that

$$\begin{aligned} \mathbf{V}^T\mathbf{K}\mathbf{V} &= \Omega \\ \mathbf{V}^T\mathbf{M}\mathbf{V} &= \mathbf{I} \end{aligned} \tag{2}$$

the flexibility matrix then can be represented with the modal parameters [3]:

$$\mathbf{F} = \mathbf{K}^{-1} = \mathbf{V}\Omega^{-1}\mathbf{V}^T \tag{3}$$

where Ω is the diagonal eigenvalue matrix and $\mathbf{V}$ is the corresponding eigenvector (modal vector) matrix. In most experimental modal analyses, only a few lower modal frequencies and modal vectors are identified. For this case, the flexibility matrix is divided into the *modal flexibility*, which is formed from the estimated frequencies and modal vectors, and the *residual flexibility* formed from the residual modes [3]:

$$\mathbf{F} = \mathbf{F}_m + \mathbf{F}_r = \mathbf{V}_m\Omega_m^{-1}\mathbf{V}_m^T + \mathbf{V}_r\Omega_r^{-1}\mathbf{V}_r^T \tag{4}$$

where the subscript m and r denote the estimated and residual quantities, respectively. Here, the modal flexibility matrix is constructed only from the measured natural frequencies and modal vectors ($\mathbf{F}_m = \mathbf{V}_m\Omega_m^{-1}\mathbf{V}_m^t$). The residual flexibility is the contribution of the unmeasured dynamic modes to the full flexibility matrix. Note that the contribution of lower modes, which are normally estimated in experimental modal analyses, are more significant than those of higher modes because the contribution of each mode is inversely proportional to the magnitude of the corresponding natural frequencies.

[1] The program is available for download from http://esaea-www.esa.lanl.gov/damage_id.

From the modal flexibility matrix $\mathbf{F}_m$ and the analytical mass matrix $\mathbf{M}$, the first Ritz vector cab be computed as:

$$\bar{\mathbf{r}}_1 = \mathbf{F}_m \mathbf{f}(s) \tag{5}$$

where $\mathbf{f}(s)$ is the spatial load distribution vector defined in Equation (1). The first Ritz vector is, then, mass-normalized as:

$$\mathbf{r}_1 = \frac{\tilde{\mathbf{r}}_1}{[\tilde{\mathbf{r}}_1^T \mathbf{M} \tilde{\mathbf{r}}_1]^{\frac{1}{2}}} \tag{6}$$

The following Ritz vectors are recursively generated. Assuming the mass matrix times the previous Ritz vector $\mathbf{M}\mathbf{r}_{s-1}$ as a load, the recurrence relationship computes the next Ritz vector $\bar{\mathbf{r}}_s$:

$$\bar{\mathbf{r}}_s = \mathbf{F}_m \mathbf{M} \mathbf{r}_{s-1} \tag{7}$$

The linear independence of Ritz vectors is achieved using the Gram-Schmidt orthogonalization:

$$\tilde{\mathbf{r}}_s = \bar{\mathbf{r}}_s - \sum_{t=1}^{s-1} (\mathbf{r}_t^T \mathbf{M} \bar{\mathbf{r}}_s) \mathbf{r}_t \tag{8}$$

Finally, the current Ritz vector is mass-normalized:

$$\mathbf{r}_s = \frac{\tilde{\mathbf{r}}_s}{[\tilde{\mathbf{r}}_s^T \mathbf{M} \tilde{\mathbf{r}}_s]^{\frac{1}{2}}} \tag{9}$$

It is worth while to compare the flexibility based extraction procedure with the state-space Based procedure proposed by Cao and Zimmerman [2]. Since the spatial load distribution vector $\mathbf{f}(s)$ in Equation (5) can be assigned arbitrary, the flexibility based method is able to generate different sets of Ritz vectors. On the other hand, influence matrix $\mathbf{B}$ estimated from the experimental modal analysis retains the information of the actual load pattern used in the modal test. Therefore, the state-space based method only identifies the Ritz vectors corresponding to the specific excitation pattern used in the actual modal testing. Note that both methods require an appropriate approximation for the mass matrix. However, since stiffness changes are the main concern of damage detection, the exact estimation of the mass matrix is not necessary.

4 ANALYTICAL MODELING

A finite element (FE) model is constructed using twenty three-dimensional beam elements. As shown in Figure 2, a girder between two nodes or cross beam is modeled as a single member. An elastic modulus of 2.0×10^5 MPa, a mass density of 7850 kg/m^3, and a Poisson's ratio of 0.2 are specified in this model. Since the accelerometers measure only the vertical movement of the structure, the lateral DOFs are not included in the analytical model. Therefore, each node of an element has two translational DOFs and three rotational DOFs. The model has a total of 64 DOFs including four rotational DOFs at the boundary. Both ends of the beam are modeled as simple pinned connections. A pinned connection is modeled by a ball bearing with a 35mm diameter in the experimental setup. Based on a preliminary vibration test, the boundary conditions appear to be less accurately modeled. The boundary conditions are then modified by introducing rotational springs at the rotational DOFs. Furthermore, additional springs are added to the rotational DOFs at both end of the cross beams to simulate the bolted connection between the girders and the cross beams. After these modifications, the relative errors of the first six natural frequencies between the analytical model and the test structure fall within 4%.

TABLE 1: Comparion of the analytical and experimental natural frequencies

Mode	Frequency (Hz)		Relative
	Ana. (ω)	Exp. ($\hat{\omega}$)	Error* (%)
1st Bending	5.45	5.56	2.06
1st Torsion	10.15	10.04	1.08
2nd Bending	19.18	18.64	2.91
2nd Torsion	30.62	29.44	4.02
3rd Bending	41.61	42.59	2.31
3rd Torsion	54.97	57.19	3.88

* error=$|\omega - \hat{\omega}|/\hat{\omega}$

Table 1 compares the values of the analytical and experimental natural frequencies. Here, the experimental frequency ($\hat{\omega}$) is a mean value of the three frequencies estimated with impacts on nodes 3, 4 and 5, respectively. Figure 3 displays the analytical and experimental modal vectors of the first six modes. The first six Ritz vectors are also computed following the extraction procedure in Section 3. Figure 4 shows the analytical Ritz vectors and the experimental Ritz vectors with an impulse excitation at node 3. The analytical Ritz vectors in Figure 4 are computed by following the procedure in Reference 2. It should be noted that the first Ritz vector is equivalent to a deflection pattern observed when a unit load is applied to node 3.

As for the scaling of the Ritz or modal vectors, a mass-normalization is conducted. However, since the DOFs of the analytical model do not coincide with the DOFs of the experimental Ritz or modal vectors, a reduced analytical mass matrix is first computed using the Guyan (static) condensation calculation. Then, both the analytical and experimental vectors are normalized with respect to the reduced mass matrix. Errors arise from the model reduction are found to be minimum since the inertial forces associated with the omitted rotational DOFs (slave DOFs) are negligible in this example.

5 APPLICATION TO DAMAGE DETECTION

A Bayesian framework is applied to diagnose the damages imposed to the test structure [10]. For an analytical model with N_{sub} substructures, the system stiffness matrix $\mathbf{K}$ can be

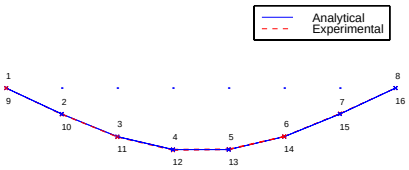

(a) The first mode

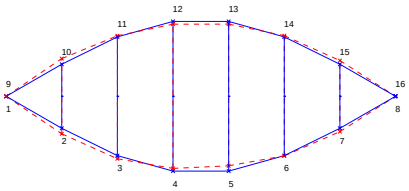

(b) The second mode

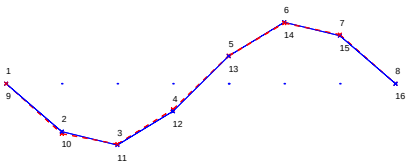

(c) The third mode

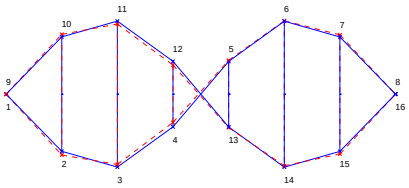

(d) The fourth mode

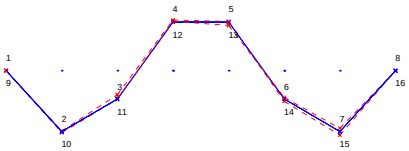

(e) The fifth mode

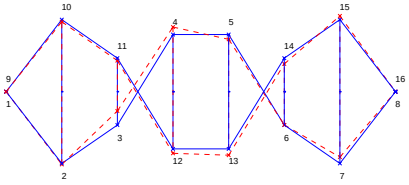

(f) The sixth mode

Figure 3: Analytial & experimental modal vectors

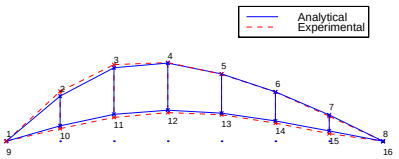

(a) The first Ritz vector

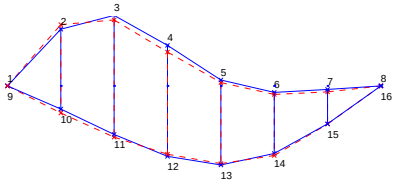

(b) The second Ritz vector

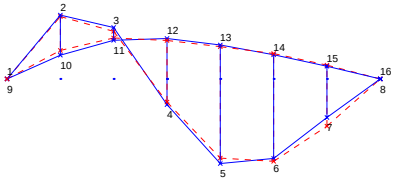

(c) The third Ritz vector

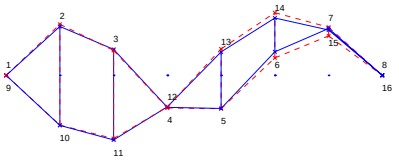

(d) The fourth Ritz vector

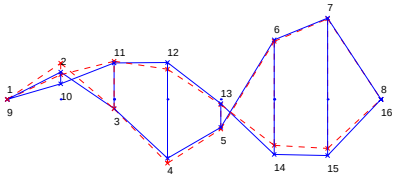

(e) The fifth Ritz vector

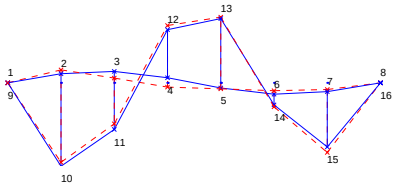

(f) The sixth Ritz vector

Figure 4: Analytical & experimental Ritz vectors

expressed as an assembly of substructure stiffness matrices $\mathbf{K}_{si}$:

$$\mathbf{K}(\Theta) = \sum_{i=1}^{N_{sub}} \theta_i \mathbf{K}_{si} \tag{10}$$

where $\Theta = \{\theta_i; i = 1, ..., N_{sub}\}$ and θ_i $(0 \leq \theta_i \leq 1)$ is a nondimensional parameter which represents the contribution of the ith substructure stiffness to the system stiffness matrix. A substructure is defined as *damaged* when the θ value is less than a specified threshold.

When vibration tests are repeated N_s times, the total collection of N_s data sets is denoted as:

$$\hat{\Psi}_{N_s} = \{\hat{\psi}(n) \ : \ n = 1, ..., N_s\} \tag{11}$$

Each data set $\hat{\psi}(n)$ is composed of the Ritz vectors estimated from the nth vibration test:

$$\hat{\psi}(n) = \left[\hat{\mathbf{r}}_1^{n\,T}, ..., \hat{\mathbf{r}}_{N_r}^{n\,T}\right]^T \in \mathbf{R}^{N_t} \tag{12}$$

where $\hat{\mathbf{r}}_i^n$ denotes the ith estimated Ritz vector in the nth data set $\hat{\psi}(n)$. The Ritz vector $\hat{\mathbf{r}}_i^n$ $(\hat{\mathbf{r}}_i^n \in \mathbf{R}^{N_d})$ has components corresponding to the instrumented DOFs. The variables N_t, N_d and N_r represent the total number of components in a data set $\hat{\psi}(n)$, the number of the measured DOFs and the number of the estimated Ritz vectors, respectively.

Let H_j denote a hypothesis for a damage event which can contain any number of substructures as damaged. The initial degree of belief about the hypothesis H_j is represented by a prior probability $P(H_j)$. Using Bayes Theorem, the posterior probability $P(H_j|\hat{\Psi}_{N_s})$, after observing the estimated data sets $\hat{\Psi}_{N_s}$, is given as:

$$P(H_j|\hat{\Psi}_{N_s}) = \frac{P(\hat{\Psi}_{N_s}|H_j)}{P(\hat{\Psi}_{N_s})} P(H_j) \tag{13}$$

The most likely damaged substructures are the ones included in the hypothesis H_{max} which has the largest posterior probability, i.e.

$$P(H_{max}|\hat{\Psi}_{N_s}) = \max_{\forall H_j} P(H_j|\hat{\Psi}_{N_s}) \tag{14}$$

Since the objective is to determine the most probable damage hypothesis (event), only the relative posterior probabilities of alternative hypotheses are of interest. We attempt to avoid the explicit expression of a posterior probability $P(H_j|\hat{\Psi}_{N_s})$ since the precise calculation of $P(\hat{\Psi}_{N_s}|H_j)$ is a difficult task. To overcome these difficulties, we focus on the relative comparisons of posterior probabilities.

Note that the search of the most likely damage hypothesis in Equation (14) theoretically requires the examination of all possible damage scenarios. We have proposed a branch-and-bound search scheme using bounding heuristics to expedite the search without exhaustively examining all the possible damage hypotheses [10]. If the damages are localized in a few substructures, the number of damage hypotheses that need to be examined by the branch-and-bound search is relatively small and the search becomes computationally feasible.

Figure 5: Actual damage introduced to the grid-type bridge structure

TABLE 2: Discription for six damage cases of a grid-type bridge structure

Case	Location 1*	Location 2*	Location 3*
1	2.0 cm (40%)	-	-
2	3.0 cm (60%)	-	-
3	3.0 cm (60%)	1.5 cm (30%)	-
4	3.0 cm (60%)	2.6 cm (52%)	-
5	3.0 cm (60%)	3.2 cm (64%)	-
6	3.0 cm (60%)	3.2 cm (64%)	2.5 cm (50%)

* Damage locations 1, 2 & 3 are shown in Figure 2. The first number is the depth of cut and the second number is the ratio of the cut depth to the height of the beam (5 cm).

Continuous deterioration of stiffness is simulated at three different regions of the grid structure and the vibration tests are conducted at six different damage stages as shown in Table 2. Figure 2 shows the three damage locations. First, a single damage is introduced at damage location 1 (for cases 1 and 2) and the second damage is formed between nodes 12 and 13 (for cases 3, 4 and 5). Finally, damage case 6 is simulated by adding damage location 3.

For each damage location, a crack is introduced by a saw cutting at a distance of 30cm from the left node. A typical saw cutting is shown in Figure 5. For example, the damage location 1 in Figure 2 is formed at 30cm left to the node 3. The severity of saw cutting in terms of depth (cm) and the ratio of the cut depth to the height of the beam (%) are tabulated as shown in Table 2. In addition, Table 3 summarizes the change of frequencies at each damage stage.

TABLE 3: Natural frequencies (Hz) estimated at different damage levels

Case	Natural Frequency (Hz)					
	1st	2nd	3rd	4th	5th	6th
0	5.56	10.04	18.64	29.44	42.59	57.19
1	5.53	9.81	18.06	29.04	42.03	56.62
2	5.48	9.67	17.27	28.50	41.18	56.18
3	5.37	9.60	17.24	27.69	40.61	55.39
4	5.24	9.52	17.22	27.34	39.77	52.40
5	5.03	9.39	17.17	27.16	38.59	51.64
6	4.96	9.01	16.18	26.70	37.29	49.95

TABLE 4: Diagnosis results for the grid-type structure using Ritz and modal vectors

	Damage	Ritz Vectors		Modal Vectors	
Case	Location	$\hat{L}_{dam}$	Rank[1]	$\hat{L}_{dam}$	Rank[1]
1	{2}	{2, 3}	1(2)	{2, 8, 9}	1(29)
2	{2}	{2, 3}	1(12)	{2, 8, 12}	1(46)
3	{2, 11}	{2, 3}	3(9)	{2, 3, 8}	13(41)
4	{2, 11}	{2}	3(3)	{2, 8, 12}	4(12)
5	{2, 11}	{2, 11}	1(1)	{2, 11, 12}	1(9)
6	{2, 6, 11}	{2, 6, 11}	1(1)	{2, 6, 11}	1(1)

1. The first number is the highest rank of a damage event which includes all actual damage locations and the second number is the rank of the actual damage event.
2. $\hat{L}_{dam}$ is a set of the most probable damage locations identified by the branch-and- bound search.

First, damage diagnosis is conducted using the six estimated modes. For each damage stage, three sets of modal data, which are obtained from the impulse excitation at nodes 3, 4 and 5, are employed for the proposed Bayesian approach. The diagnosis results are summarized in Table 4. The fifth column of the table (the column under $\hat{L}_{dam}$) shows the most likely damage locations identified by the branch-and-bound search scheme. The first number under the title "*Rank*" denotes the highest rank among the damage events that include all the actual damage locations and the second number presents the rank of the actual damage event. The diagnosis results reveal that as we approach to the final damage stage, the diagnosis employing the modal parameters converges to the actual damage locations.

Second, the same six cases are re-diagnosed using the Ritz vectors generated from different load patterns. A point load is assumed to be applied to the vertical direction of each node and the first six Ritz vectors are generated from the load pattern. Then, this process is repeated for all twelve vertical DOFs. From these load patterns, a total of 72 (6 Ritz vectors/load $\times$ 12 load patterns) Ritz vectors are generated. Note that, following the proposed extraction procedure, Ritz vectors corresponding to any load pattern can be theoretically extracted with the same amount of test data used to estimate the modal parameters. That is, more information is gained by applying multiple loads.

The diagnosis results using the Ritz vectors are also summarized in Table 4. For cases 1 and 2, the actual damage event is ranked as the second and twelfth most likely damage event, respectively. In the first two cases, damage location 1 is included in the most likely damage event estimated by the branch-and-bound search. This is, although the branch-and-bound search fails to pinpoint the actual damage location, the search finds the actual damage location as one of the most likely damage locations. For case 3, the actual damage event is ranked as the ninth most likely event. For case 4, the actual damage case is ranked as the third most likely event. For cases 5 and 6, the branch-and-bound search exactly finds the actual damage events.

TABLE 5: Diagnosis result for damage case 3 of the girder structure

Rank	$\hat{L}_{dam}$	Rank	$\hat{L}_{dam}$	Rank	$\hat{L}_{dam}$
1	{2, 3 }	4	{2, 3, 12}	7	{1, 2, 3}
2	{2, 3, 4}	5	{2 }	8	{2, 12 }
3	{2, 3, 11}	6	{2, 4 }	9	{2, 11 }

Table 5 shows the first nine most probable damage events identified by the branch-and-bound search for damage case 3. The first two most probable events only include damage location 1 and miss damage location 2. However, the third most probable event includes the two damage locations and one extra member 3. That is, although the proposed approach ranks the actual damage event as the ninth most probable event, the third most likely event conservatively includes all the actual damage locations.

The results shown in Table 4 indicates that the Ritz vectors provide better diagnosis results for the six damage cases investigated than the modal vectors. The sensitivity comparison shown in Figure 6 supports the diagnosis results. In Figure 6, the sensitivity comparison using the experimental Ritz/modal vectors at different damage stages is conducted. The Ritz vectors are extracted from a point load applied at node 3. From Figure 6, we conclude that a careful selection of load patterns can make damages more observable. The better sensitivity of Ritz vectors to damage locations and the increased amount of information employing multiple load patterns seem to improve the damage diagnosis.

6 SUMMARY AND DISCUSSIONS

In this paper, load-dependent Ritz vectors are incorporated into the previously proposed Bayesian framework for damage diagnosis. We also describe a new procedure which extracts Ritz vectors based on the measured flexibility matrix. The

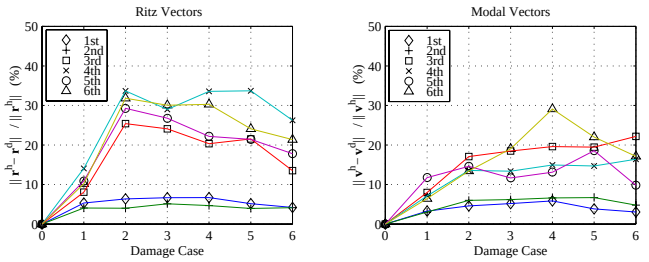

Figure 6: Sensitivity of Ritz and modal vectors at different damage stages

main advantage of the flexibility based extraction procedure is that the method can generate Ritz vectors from arbitrary load patterns. Damage diagnoses of the grid-type bridge model indicate that the employment of Ritz vectors provides better indication of the actual damage locations. The superior performance of Ritz vectors over modal vectors attributes to (1) the better sensitivity of Ritz vectors over modal vectors and (2) the increased amount of information obtained by employing multiple load patterns.

ACKNOWLEDGMENTS

This research is partially sponsored by the National Science Foundation under Grant No. CMS-95261-2. The authors wish to express their sincere thanks to Hyundai Engineering & Construction Co. LTD. for inviting the first author to participate in the test of the grid-type bridge model, and to Dr. Chuck R. Farrar and Dr. Scott W. Doebling of the Los Alamos National Laboratory for providing the DIAMOND software.

REFERENCES

[1] T. T. Cao and D. C. Zimmerman. Application of load-dependent Ritz vectors in structural damage detection. In *Proceedings of the 15th International Modal Analysis Conference*, pages 1319–1324, Orlando, FL, 1997.

[2] T. T. Cao and D. C. Zimmerman. A procedure to extract Ritz vectors from dynamic testing data. In *Proceedings of the 15th International Modal Analysis Conference*, pages 1036–1042, Orlando, FL, 1997.

[3] S. W. Doebling. *Measurement of Structural Flexibility Matrices for Experiments with Incomplete Reciprocity*. PhD thesis, Aerospace Engineering Sciences, University of Colorado, Boulder, CO, 1995.

[4] S. W. Doebling, C. R. Farrar, M. B. Prime, and D. W. Shevitz. Damage identification and health monitoring of structural and mechanical systems from changes in their vibration characteristics: A literature review. Technical Report LA-13070-MS, Los Alamos National Laboratory, Los Alamos, NM, 1996.

[5] C. R. Farrar and K. M. Cone. Vibration testing of the I-40 bridge before and after the introduction of damage. In *Proceedings of the 13th International Modal Analysis Conference*, pages 203–209, Nashville, TN, 1995.

[6] C. R. Farrar, S. W. Doebling, P. J. Cornwell, and E. G. Straser. Variability of modal parameters measured on the Alamosa Canyon Bridge. In *Proceedings of the 15th International Modal Analysis Conference*, pages 257–263, Orlando, FL, 1997.

[7] T. A-L. Kashangaki, S. W. Smith, and T. W. Lim. Underlying modal data issues for detecting damage in truss structures. Technical Report AIAA-92-2264-CP, American Institute of Aeronautics and Astronautics, 1992.

[8] H. M. Kim and R. R. Craig. Application of unsymmetric block Lanczos vectors in system identifications. *International Journal of Analytical and Experimental Modal Analysis*, 7:227–241, 1992.

[9] A. K. Pandey, M. Biswas, and M. M. Samman. Damage detection from changes on curvature mode shapes. *Journal of Sound and Vibration*, 145:321–332, 1991.

[10] H. Sohn and K. H. Law. Bayesian probabilistic approach for structure damage detection. *Earthquake Engineering and Structural Dynamics*, 26:1259–1281, 1997.

[11] H. Sohn and K. H. Law. Application of load-dependent Ritz vectors to Bayesian probabilistic damage detection. *Probabilistic Engineering Mechanics*, 1999. (in print).

[12] N. Stubbs, J. T. Kim, and K. Topole. An efficient and robust algorithm for damage localization in offshore platforms. In *ASCE Tenth Structures Congress*, pages 543–546, San Antonio, TX, 1992.

[13] G. C. Yao, K. C. Chang, and G. C. Lee. Damage diagnosis of steel frames using vibrational signature analysis. *Journal of Engineering Mechanics, ASCE*, 118:1949–1961, 1992.